Available online at www.sciencedirect.com
SCIENCE DIRECT®
Journal of Nuclear Materials 336 (2005) 243–250
journal of nuclear materials
www.elsevier.com/locate/jnucmat

Electrical behavior of platinum-group metals in glass-forming oxide melts

C. Simonnet [a,*], A. Grandjean [b], J. Phalippou [a]

[a] Laboratoire des Verres, Université Montpellier II, CC. 69, Place Eugène Bataillon, 34095 Montpellier cedex 5, France
[b] CEA Marcoule Valrhô, DEN/DTCD/SCDV/LEBV, BP. 17171, 30207 Bagnols sur Cèze cedex, France

Received 18 May 2004; accepted 21 September 2004

Abstract

This paper presents an experimental study of the electrical conduction mechanisms in glass-forming oxide melts containing RuO_2 needles. The composites were obtained by melting calcine in an industrial-scale induction-heated cold crucible melter. The temperature dependence of the conductance was measured by complex impedance spectroscopy, using a four-electrode cell, from 1200 °C to 400 °C. Direct current analysis revealed that even with low RuO_2 content, electronic and ionic transport occurred over a wide temperature range. The RuO_2 particle dispersion significantly enhances the total electrical conductivity up to 1200 °C. Percolation theory associated with tunneling conduction models is used to describe the electronic contribution to the conductivity. An equivalent circuit is proposed to describe the mixed ionic–electronic transport. The electronic conductivity not only depends on the RuO_2 content, but on the particle length-to-diameter ratio and the RuO_2 solubility.

PACS: 72.80.N; 72.60

1. Introduction

Platinum group metals are chemically stable up to high temperatures and are not corroded by molten borosilicates. Investigations into the noble metal behavior in glass melting processes show that the metals have limited solubility on the order of 100 ppm [1,2]. In the nuclear field, the properties of the fission by-products including the platinoids Ru, Rh, and Pd in glass melts have been investigated because they significantly affect the viscosity and the thermal and electrical properties of the melt during vitrification processes [3,4].

Two types of platinum-group metal particles are found in borosilicate nuclear waste glasses. The palladium and rhodium species form spherical $PdRh_xTe_y$ alloys with tellurium. The ruthenium species precipitate and crystallize into long, needle-like RuO_2 particles [5]. The RuO_2 rutile phase is dense ($\rho = 6.97\,g/cm^3$) and metallic conductive ($\sigma = 2.5 \times 10^4\,\Omega^{-1}\,cm^{-1}$). In typical HLLW glasses, the platinoid (Ru, Rh, Pd) phases account for ~0.5 vol.%, but their agglomeration and sedimentation result in the formation of layers of higher content, the viscosity and electrical conductivity of which can increase by an order of magnitude [6].

The electrical conduction and viscosity gradients significantly diminish the efficiency of the melting process, both in the Induction Heated Melter with cold crucible or in the Liquid-Fed Ceramic Melter with electrodes

* Corresponding author.
E-mail address: simonnet@univ-montp2.fr (C. Simonnet).

0022-3115/$ - see front matter © 2004 Published by Elsevier B.V.
doi:10.1016/j.jnucmat.2004.09.019

[4,5]. Despite their technical importance in these processes, electrical transport mechanisms in molten borosilicates containing platinum-group particles have still not been fully elucidated. In the area of microelectronic components, electrical transport has been widely investigated in high-lead glasses containing RuO_2 particles, known as TFR [7–9].

Many conduction mechanism models have been proposed in the literature concerning electrical transport in these composites. Above a very low critical RuO_2 content, electronic transport occurs and the conductivity increases with the RuO_2 content [9]. Although this is still a subject for debate among thick-film researchers, the electrical percolation model [10] and the tunneling barrier model [7] seem to best match the experimental results.

The literature on the electrical transport in noble-metal/glass heterogeneous materials suggests that only the metal oxide phase RuO_2 can play an important role in the electronic transport at low content. This is consistent with the fact that, unlike the metal or alloy phases, the RuO_2 phase has outstanding properties. The RuO_2 phase exhibits unique redox properties. The Ru^{2+}, Ru^{3+} and Ru^{4+} defects at the rutile surface are likely to adsorb mobile cations (like H^+, Li^+, Na^+) and/or enhance electron transfer across the RuO_2 /glass interface [11]. Moreover, the RuO_2 phase has an outstanding interaction with glass. Some authors have suggested the presence of subtle structural modifications in the very thin area across the RuO_2/glass interface [12]. In glass-forming molten oxides, the RuO_2 particles tend to agglomerate with interparticle distance typically on the order of 1 nm. This equilibrium distance could be the consequence of a competition between van der Waals attraction forces and 'steric-like' or electrostatic repulsion forces [13].

At the melting temperature (~1200 °C), as the solubility of the platinum-group metals is very low, the mass concentrations of the soluble species in the molten borosilicate are negligible compared to those in the metal and the metal oxide phases. The material studied consists of a complex molten borosilicate containing metallic alloy spheres and RuO_2 needles. Laboratory-scale investigations have revealed that at about 2 wt% platinoid content, the electrical conductivity increases significantly whereas the viscosity remains nearly unchanged [6]. The authors have suggested that the electrical conductivity depends on the size and the morphology of the RuO_2 particles, but they have not proposed electrical transport mechanisms to explain the abnormally high electrical conductivity.

In a recent work, we have studied the electrical properties of molten borosilicates containing RuO_2 particles by changing the morphology of the particles (needles or grains) and the nature of the matrix (good or poor ionic-conducting matrix) [14]. The results have revealed that these heterogeneous materials are mixed ionic–electronic conductors. The electronic contribution to the conductivity does not depend on the nature of the matrix, but to a large extent on the microstructure of the particle network, which is consistent with the electrical percolation model. However, the electrical transport mechanisms have not been fully elucidated.

The present work focuses on the electrical conduction mechanisms in simulated HLLW glass melts. The experimental data are used to determine the critical RuO_2 content above which electronic transport occurs, and the conductivity versus RuO_2 content relation. We then discuss the electronic transport mechanism that implies the interparticle electronic jump.

2. Experimental

2.1. Glass preparation

The compositions studied simulated a complex nuclear waste glass containing noble metals. In these glasses, platinoid phases as Pd, Rh and RuO_2 typically account for 0.1, 0.04 and 0.4 vol.%, respectively. As RuO_2 is assumed to be mainly responsible for the outstanding electrical behavior of oxide melts, we only considered the RuO_2 content. The compositions were then called MATRIX(x) where MATRIX is the name of the noble-metal free glass and x is the volume percent of the RuO_2 phase.

A complex composite IHM(0.7) was prepared by industrial-scale vitrification of simulated high-level waste in Induction-Heated Melter. The RuO_2 phase, present as needles, accounted for 0.7 vol.% of the composite (Fig. 1). The needle length ranged from 10 μm to 20 μm. The aspect ratio (length-to-diameter ratio)

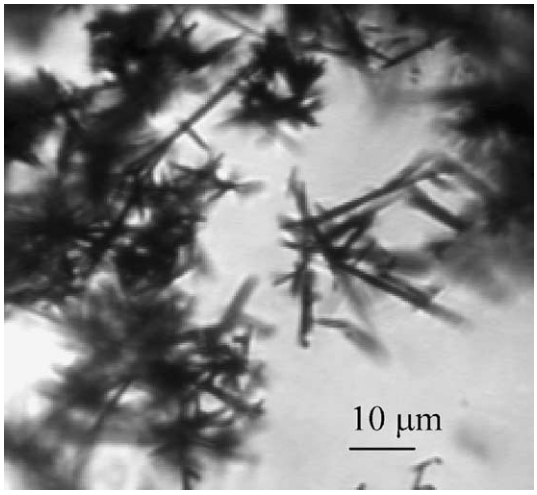

Fig. 1. Optical microscope (transmission) image of RuO_2 needles in IHMn(0.7).

was about 10:1. Higher concentrations (IHM(x), $x > 0.7$ vol.%), as well as the noble-metal free IHM matrix, were obtained by particle sedimentation during heat treatment. The RuO_2 content was determined by density measurements using the Archimedes principle.

Some results obtained by Luckscheiter [6] on a simulated nuclear waste glass containing RuO_2 needles (LUCK(x)) were also reported.

2.2. AC impedance analysis

For the electrical conductivity measurements, the composite was ground and a suitable amount (≈35 g) was remelted in an alumina crucible placed in the homogeneously heated zone of a tubular furnace. Details of the experimental setup, calibration, and corrections for the four-electrode measurements have been described elsewhere [15]. The sample conductivity was measured between 1200 °C and 400 °C. The upper limit of the temperature range was chosen to minimize aggregation or sedimentation phenomena.

The electrical conductivity changes were followed by impedance spectroscopy measurements in 10 °C steps as the melt cooled. The Nyquist diagram was plotted at each temperature. The sample resistance R was extracted and the electrical conductivity was determined using the relation $\sigma = K/R$, where K is the cell constant. An aqueous KCl solution with conductivity in the range of that of the molten sample was used to evaluate K. A few electrical conductivity measurements were performed during the second heating run of the composite. The furnace was stabilized at each temperature step for the reheating measurements.

2.3. Direct current analysis

The purpose of the present method is to allow the determination of the partial electronic (electron/hole) conductivity of a mixed ionic–electronic conductor. This time-domain measurement aims at emphasizing electrode polarization in order to block ionic diffusion. It required a two-blocking electrode configuration, which consisted in the two external sheets of the four-electrode cell. The melt was stabilized at each temperature T studied. The sample was provided with a voltage step ΔV of amplitude $V_i = 0.15$ V for the duration t_d, of 1 ms to infinity, and the current $i(t)$ was detected as the output voltage $U(t)$ across a reference resistor R_{ref} (Fig. 2). The voltage variations across the electrodes $V_r(t)$ were also measured. Assuming that no electrolysis, or charge transfer, occurs at the electrodes, the current increases instantaneously with the ΔV and decreases exponentially with the piling-up of ions at the electrodes. When the mobility of ions increases (at high temperatures), the exponential decay leads to a null ionic current in a few milliseconds. Electronic transport is assumed to be responsible for the remaining steady currents. This method is based on the hypothesis of independent ion and electron transport mechanisms.

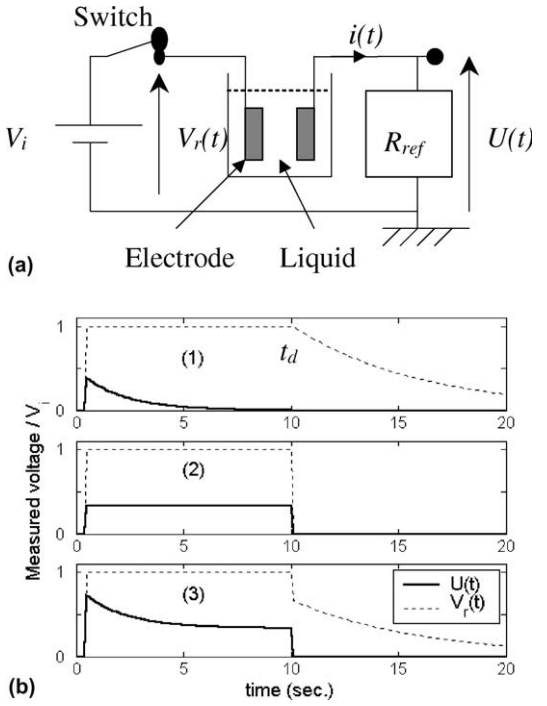

Fig. 2. (a) Schematic illustration of the dc experiments. (b) Single-shot responses of (1) a purely ionic-conducting liquid, (2) a purely electronic-conducting liquid, and (3) a mixed ionic–electronic conducting liquid.

3. Results and discussion

The IHM matrix contains more than 20 elements but its electrical properties are mainly those of a simple sodium borosilicate glass (SBN). The diffusion of Na^+ is mainly responsible for the electrical transport. The ionic conductivity of the IHM matrix is comparable to that of the simple SBN matrix (Fig. 3). For both matrices, the temperature-dependence of the electrical conductivity is satisfactorily described by Arrhenius and Vogel-Tamman-Fulcher (VTF) laws, below and above T_g respectively [15]. The complex impedance plot of a purely ionic-conducting liquid like IHM shows a semicircular arc characterizing electrode polarization (Fig. 4) [15]. The melt electrical resistance is read at the high-frequency intersection of the semi-circle with the x-axis ($-Z''$ minimum).

As the RuO_2 concentration increases, the impedance plot of IHM(x) is no longer circular, but is distorted and shifted to lower (Z' values along the x-axis (Fig. 4). As we think that the frequency dispersion still corresponds

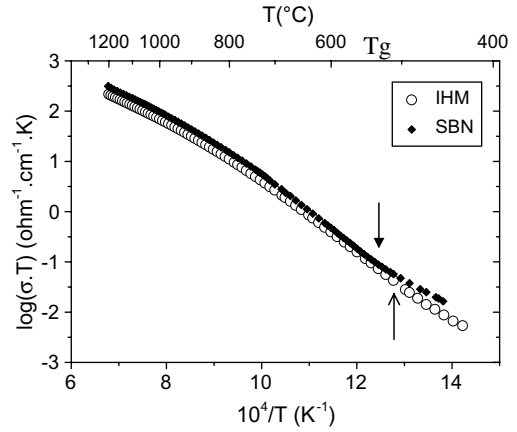

Fig. 3. Inverse temperature dependence of the electrical conductivity of the IHM matrix compared with that of a simple sodium borosilicate (SBN). The matrix (SBN) contains SiO_2, B_2O_3, Na_2O at a mass ratio of 55:30:15. For both matrices an arrow indicates the glass transition temperature.

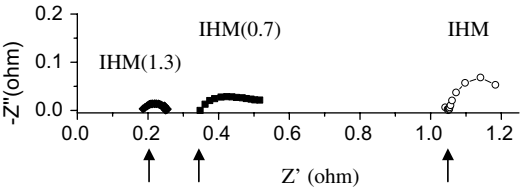

Fig. 4. Plot of $-Z''$ versus Z' for IHM, IHM(0.7) and IHM(1.3), from 1 MHz (left) to 100 Hz.

to an effect of electrode polarization, we chose, by convention, to read the resistance at the intersection of the high frequency part of the distorted 'arc' with the x-axis (see arrows).

The measurements performed during the cooling of the melt were used to extract Arrhenius plots for the IHM(x) series, within the [1200–600 °C] temperature range (Fig. 5). At a given temperature, the electrical conductivity increases significantly with the RuO_2 content. For each RuO_2 content, an 'apparent' activation energy can be calculated from the $\log(\sigma)$ versus $1/T$ plot slope. The order of magnitude of the activation energy for electrical conduction in molten IHM(x) is 1 eV. The analysis of the electrical conductivity data is not straightforward.

The dc current analyses were carried out to check the hypothesis of an electronic mechanism at molten state. As the ionic mobility is high at molten state, the accumulation of ionic carriers, i.e., the double-layer formation, lasts a few milliseconds when the voltage step is applied so that the ionic current drops to a null value. For IHM(x) melts, an electronic current was detected except for very low x values ($x < 0.2$ vol.%), which behave as IHM (not shown here). The electronic current

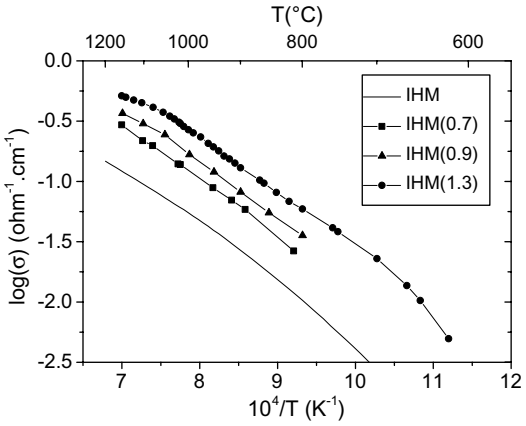

Fig. 5. Inverse temperature dependence of the electrical conductivity of the IHM(x) series.

increases as the temperature increases. Nevertheless, the electronic conductivity only accounts for a fraction of the total electrical conductivity at molten state. For IHM(1.9) at 1100 °C (Fig. 6), the electronic conductivity measured in the time domain is obtained using the value U_e of the voltage U, at the plateau. The electronic contribution is around six fold higher than the ionic conductivity of the molten IHM matrix so the electrical transport mechanism is mainly electronic.

We assume that the electronic transport is independent of the ionic transport. For low RuO_2 volume fractions, we can assume as well that the ionic conduction pathways do not significantly change. At a given temperature, we can then determine the electronic conductivity by subtracting the ionic conductivity of the molten matrix IHM from the electrical conductivity of the molten

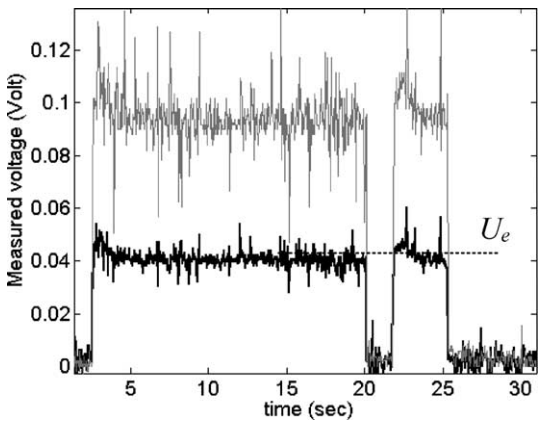

Fig. 6. Variations of the current intensity $i(t) = R_{ref} \times U(t)$ as a function of time (thick line), in response to two consecutive applied voltage steps (thin line) for the IHM(1.9) melt at 1100 °C.

IHM(x). Fig. 7 shows the RuO_2 concentration dependence of the electrical conductivity at 1150 °C. We have added to our data those obtained by Luckscheiter, LUCK(x), at the same temperature [6,14]. The electronic conductivity is comparable for both compositions.

As it has been suggested in the literature for solid RuO_2–glass composites [9,10], and recently for molten borosilicates containing RuO_2 particles [14], the electronic conduction occurs through a network of interconnected particle chains. The RuO_2 particles are separated from their neighbors on the chain by a thin matrix layer. This isolating layer acts as an interparticle barrier for electronic conduction. The electronic conductivity σ_e can be described by the relation

$$\sigma_e = \sigma_{e0}(x - x_c)^{\mu}, \quad (1)$$

where x is the RuO_2 volume fraction, x_c is the critical volume fraction corresponding to the percolation threshold and μ is the critical exponent of the scaling law. The parameters $\sigma_{e0} = 6 \times 10^3$ S/cm, $x_c = 0.15$ vol% and $\mu = 2.3$ satisfyingly fit the experimental results (Fig. 7). For comparison, the parameters corresponding to the classical percolation predictions for spherical RuO_2 particles embedded in an isolating matrix would be $\sigma_{e0} \sim 3 \times 10^4$ S/cm, $x_c \sim 15$ vol.% and $\mu = 1.7$ (Fig. 7). The particle morphology affects the critical volume fraction, which can reach values as low as 1 vol.% for needle-shaped particles of high aspect ratio [16].

The classical percolation model corresponds to an abrupt transition from isolating properties to conducting properties. It is based on the apparition of an infinite chain of conducting particles in which the neighboring particles contact one another. In the case of RuO_2–glass systems, the needle morphology is not the only relevant parameter that explains the very low percolation threshold and the abnormally high critical exponent. Very low percolation thresholds (1 vol.%) have been also found for networks of grain-shaped RuO_2 particles in borosilicate matrices [9,14].

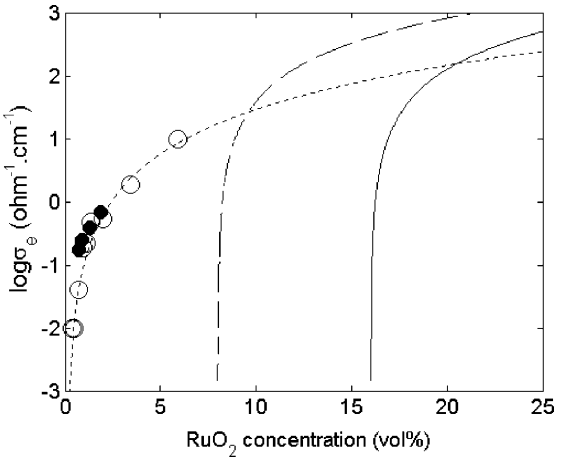

Fig. 7. Effect of RuO_2 needle concentration on the electronic conductivity of the IHM(x) series (solid circles) and LUCK(x) series (open circles) at 1150 °C. The series LUCK(x) represent the data obtained by Luckscheiter on simulated HLW melt at 1150 °C [6]. The solid line represents Eq. (1) with $\sigma_{e0} = 3 \times 10^4$ S/cm, $x_c = 15$ vol.% and $\mu = 1.7$. The dashed line represents Eq. (1) with $\sigma_{e0} = 3 \times 10^4$ S/cm, $x_c = 8$ vol.% and $\mu = 1.7$.

As it has been suggested in the literature, the RuO_2/glass interaction has outstanding characteristics. In particle agglomerates, the particles are not in contact but a thin layer of matrix separates them. The region of the closest approach between two conducting segments can be schematically depicted as a parallel-plate capacitor with area A, separation d and capacitance $C = A/4\pi d$ [7]. The thickness d is typically on the order of 1 nm for RuO_2/glass composites.

This typical equilibrium distance could be attributed to the interplay of van der Waals attraction forces and repulsion forces due to the structure of the thin intergranular liquid, as it has been suggested for liquid-sintered polycrystalline ceramics [13]. The intergranular molten borosilicate wets the RuO_2 surface. Contact angles of 50° have been measured between RuO_2 thin film and glass with a viscosity of 10^4 Pa s [17]. The crystallographic structure of the RuO_2 phase may induce a preferred epitaxial orientation of the silica liquid (SiO_4 tetrahedra) on the grain surfaces. As the liquid intergranular layer gets small, the configuration matching becomes severe and the energy of the system rises [13]. This equilibrium thickness has been observed experimentally on liquid-phase sintered ceramics [18] and on glass containing nano-sized RuO_2 grains [12]. For needle-shaped RuO_2 particles, it seems that the region of closest approach between two particles is mainly at the points. Agglomerates of RuO_2 needles seem to adopt urchin shape (Fig. 1).

The typical distance $d = 1$ nm between conducting segments is consistent with the presence of tunneling conduction mechanisms. This conduction model has been widely used in the literature to describe the electrical properties of solid RuO_2–glass composites [7]. The resistance R_e, which controls the amount of electronic current, can be expressed as a series combination of the resistance of the RuO_2 phase $R_m(T)$ and the tunneling resistance $R_b(T)$ (Fig. 8):

$$R_e(T) = \sum_{i=1}^{n} (R_{mi}(T) + R_{bi}(T)), \quad (2)$$

where i represents the basic unit of the tunneling barrier model which consists of a metal–insulator segment. The number of segments n depends on how the chain segments are connected geometrically. In particular, it depends on the particle morphology and the chain tortuosity.

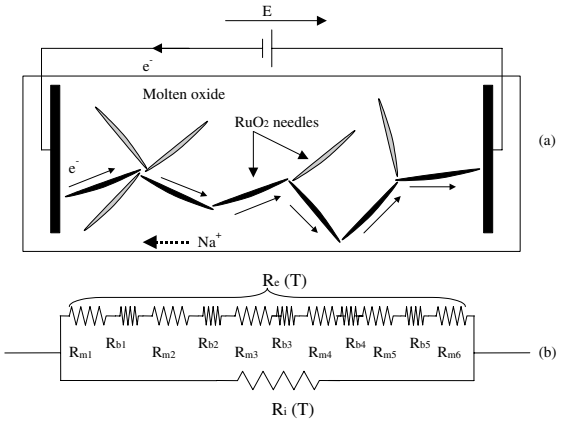

Fig. 8. Schematic representation of the electronic and ionic pathways during direct current measurements in a sodium borosilicate melt containing RuO_2 needles. Electrons move along chains of RuO_2 needles, whereas diffusion of sodium ions occurs in the oxide melt.

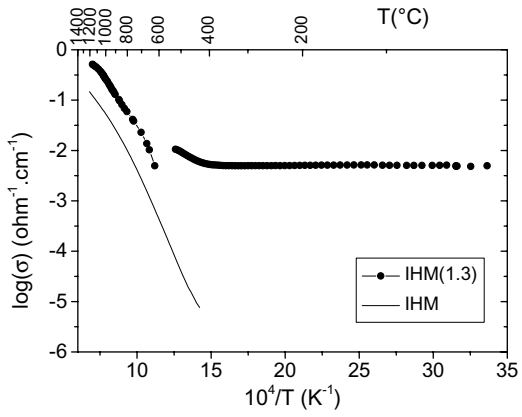

Fig. 9. Inverse temperature dependence of the electrical conductivity of the IHM(1.3) composite, from 25 °C to 530 °C (on composite disk using a two-electrode method), and from 1200 °C to 600 °C (in a crucible using the four-electrode method). The data corresponding to the IHM matrix are also reported (solid line).

The overall resistance of the heterogeneous material can be expressed as a parallel combination of the resistance of the electronic contribution, corresponding to the particle network, and the resistance of the ionic contribution, corresponding to the matrix (Fig. 8). This is valid if we assume that electronic and ionic transports are independent.

In the solid state, ac impedance analysis with the two-electrode technique [15] was performed on IHM(1.3) disks from 25 °C to the glass transition temperature (510 °C) in order to check the assumption that the ionic contribution to the electrical conductivity is negligible compared to the electronic contribution (Fig. 9). The discrepancy between the four-electrode method data and the two-electrode method data around T_g may be due to the uncertainty on the RuO_2 content in the small solid samples and to the different thermal treatments. Nevertheless, the experimental results at low temperatures confirm that the high conductivity is mainly due to electronic transport. We assume that the tunnel barrier resistance limits the amount of current that flows along a particle chain. Based on the tunneling barrier model, the overall resistance can then be expressed by the following equation:

$$R(T) = R^*_{b0} \exp(\lambda T) \left(\frac{\sin aT}{aT}\right) \left[1 + \exp\left(\frac{E}{kT}\right)\right], \qquad (3)$$

where T is the absolute temperature, a is related to the insulating barrier height, E is the electrostatic charging energy, k is Boltzmann's constant, R^*_{b0} is a lump term accounting for the barrier characteristics and the number of barriers along the conducting pathways, and λ is a term accounting for the thermal expansion of the composite. λ is proportional to the thermal expansion coefficient of the glass matrix. The barrier characteristics include the barrier thickness d and area A, the energy level V_0 and the impurity concentration within the barrier.

This expression satisfyingly describes the weak temperature dependence of the electrical conduction of composites with RuO_2 content above x_c, below the glass transition temperature. Below T_g, the barrier characteristics are assumed to be constant, except the distance d, which is expected to increase with the temperature.

Some authors have proposed that the impurity concentration within the barriers significantly affects the tunneling probability [7]. During the high-temperature processing of the heterogeneous material (firing or glass melting), the metal oxide partially dissolves in the glass. Although the reported solubility of ruthenium in borosilicate glasses is not high [1], soluble ruthenium species are present [9,19,20] and their concentration is enhanced near sharp particle edges (like the needlepoint). This hypothesis is consistent with the investigations on the growth of RuO_2 particles in molten oxides [21].

The oxidation state and the coordination of the ruthenium ions are more uncertain. Some investigations on silicate glasses doped with ruthenium ions have suggested that tetravalent ruthenium is in equilibrium with trivalent ruthenium [22,23] and that the Ru^{4+} species mainly contribute to the electronic conduction mechanism [23]. They have evidenced also that the firing conditions (the hydrogen or oxygen atmosphere) significantly affect the final electrical properties of ruthenium-doped glasses by modifying the ratio between the concentrations of Ru^{3+} and Ru^{4+} species. With all these features given in the literature, the presence of ruthenium impurities in the molten glass is hardly in question. However, the exact mechanism by which they affect the tunneling transmission coefficient is uncertain.

Some authors have proposed that ruthenium impurities act as resonant tunneling centers, which create localized energy levels accessible to the electrons [7]. We are currently unable to propose a detailed mechanism accounting for the effect of the ruthenium impurities on the tunneling properties. Nevertheless, it is clear that below the glass transition temperature, the concentration of ruthenium impurities in glass does not vary with the temperature or the time, as the structure of the material is frozen. On the contrary, above T_g, the ruthenium concentration increases with both temperature and time, as an effect of the dissolution kinetics.

In a previous work concerning simple sodium borosilicate melts containing RuO_2 grains, we have indirectly evidenced the role of the ruthenium impurities on the electronic conduction mechanism by showing that the electrical conductivity has a different pattern of behavior during cooling and heating runs of the material [14]. This hysteresis loop can also be observed with the IHM(x) melts (Fig. 10). If we assume that the tunneling occurs over the whole temperature range studied and that the ruthenium solubility is mainly responsible for the temperature dependence of the electronic conductivity above the glass transition temperature, we may get a rough idea of the solubility contribution to the tunneling probability. We report in Fig. 9 the concentration (in ppm) of the soluble ruthenium species versus $1/T$. These data have been reported in the literature [1] for sodium silicate melts with 20 mol% Na_2O. The variations of the conductivity are comparable with those of the solubility. As an example, from 900 °C to 1150 °C, both the electrical conductivity and the ruthenium solubility increase by an order of magnitude. This suggests that the tunneling current could be proportional to the concentration of ruthenium impurities within the tunneling barriers.

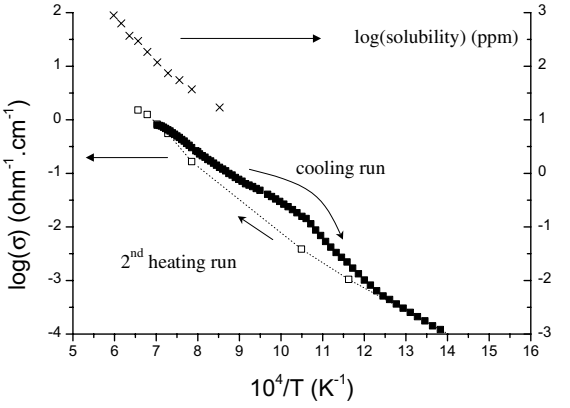

Fig. 10. Arrhenius plot of the electrical conductivity of IHM(1.9) during cooling (solid symbols) and reheating (open symbols) of the melt. For comparison, the temperature dependence of the ruthenium solubility in a sodium silicate melt is also reported (data from the literature [1]).

Although some aspects of the impurity-assisted tunneling mechanism remain unclear, we speculate that:

- The morphology of the particles is a very important parameter because it is correlated to the number of tunneling barriers along the conducting chains. At a given RuO_2 content, the electronic contribution to the conductivity should increase with the aspect ratio of the particles. On the contrary, the percolation threshold should decrease with the aspect ratio.
- The thickness of the interparticle layer significantly affects the tunneling probability. To minimize electronic conduction, one should work out a matrix composition that increases the repulsion forces between RuO_2 particles. Some authors have suggested that the presence of titanium in the matrix would increase the interparticle distance [24].
- The composition of the matrix should play an indirect but important role on the electrical properties. It has been observed that both the aspect ratio of the particles [25] and the ruthenium solubility [1] increase with the Na_2O content. Both effects enhance the electrical conduction. The redox properties of the melt should affect the electronic conduction by controlling the equilibrium concentration ratio of the soluble impurities Ru^{3+} and Ru^{4+}.
- The temperature and the duration of the melting process should affect the electronic conductivity. The high temperatures enhance the ruthenium solubility and are suspected to favor high aspect ratios. Long duration involves aggregation and sedimentation, which increase the RuO_2 content in localized molten mass zones. The areas of high RuO_2 content should show higher conductivity. This should result in localized overheating. The continuous stirring of the melt should prevent this unstable heterogeneous heating.

Lastly, we would like to stress the point that the critical fraction $x_c = 0.15$ vol.% found by fitting the electronic conductivity versus the RuO_2 content curve corresponds to the apparition of a conducting pathway for electronic transport. At this content, the electronic contribution to the conductivity is negligible compared with the ionic contribution to the conductivity. The content at which the electronic conductivity is on the order of the ionic conductivity is closer to 0.4 vol.%.

The study on the correlation between the ruthenium impurity concentration and the tunneling current is now in progress.

4. Conclusion

Four-electrode impedance spectroscopy was used to determine both the temperature- and the RuO_2 content-dependence of the electrical conductivity of

simulated nuclear oxide melts. Using the direct current method, we showed that electronic transport is responsible for the abnormally high electrical conductivity, for RuO_2 content as low as 0.4 vol.%. The variations of the electronic conductivity with the RuO_2 content are understandable in light of electrical percolation considerations. In light of the literature on RuO_2–glass composites, we propose that the limiting mechanism on electronic transport is the tunneling through insulating interparticle barriers, even at high temperatures. Above the glass transition temperature, the increasing ruthenium solubility involves the 'doping' of the matrix layer with ruthenium impurities. We propose that these impurities enhance the tunneling current and consequently the electrical conductivity. We then give reasonable predictions on how the electrical conductivity of oxide melts containing platinum-group particles could be affected by the RuO_2 content, the organization of the RuO_2 particle network, the size and the morphology of the RuO_2 particles and the ruthenium solubility.

References

[1] J. Mukerji, S.R. Biswas, Cent. Glass. Ceram. Res. Inst. Bull. 14 (2) (1967) 30.
[2] T. Akai, J. Nishii, M. Yamashita, H. Yamanaka, J. Non-Cryst. Solids 222 (1997) 304.
[3] H. Mitamura, T. Murakami, T. Banda, J. Nucl. Mater. 136 (2) (1985) 104.
[4] A.V. Demin, Y.I. Matyunin, M.I. Fedorova, Proceedings of the Vth International Conference on Radioactive Waste Management and Environmental Remediation, Berlin, Germany, Vol. 1, ASME, New York, 1995, p. 443.
[5] C. Krause, B. Luckscheiter, J. Mater. Res. 6 (12) (1991) 2535.
[6] B. Luckscheiter, in: Proceedings of the 1993 International Conference on Nuclear Waste Management and Environment Remediation, Vol. 1, Prague, Czech Republic, 1993, p. 427.
[7] G.E. Pike, C.H. Seager, J. Appl. Phys. 48 (1977) 5152.
[8] O. Abe, Y. Taketa, J. Phys. D: Appl. Phys. 24 (1991) 1163.
[9] T. Yamaguchi, Y. Nakamura, J. Am. Ceram. Soc. 78 (5) (1995) 1372.
[10] P.J.S. Ewen, J.M. Roberston, J. Phys. D: Appl. Phys. 14 (1981) 2253.
[11] L.M. Doubova, S. Daolio, A. De Battisti, J. Electroanal. Chem. 532 (2002) 25.
[12] K. Adachi, S. Iida, J. Ishigame, S. Sekihara, J. Mater. Res. 6 (8) (1991) 1729.
[13] D.R. Clarke, J. Am. Ceram. Soc. 70 (1) (1987) 15.
[14] C. Simonnet, A. Grandjean, J. Non-Cryst. Solids, submitted for publication.
[15] C. Simonnet, J. Phalippou, M. Malki, A. Grandjean, Rev. Sci. Instrum. 74 (5) (2003) 2805.
[16] J. Vilcakova, P. Saha, O. Quadrat, Euro. Polym. J. 38 (2002) 2343.
[17] A. Honda, S. Watanabe, H. Takagi, Y. Sakabe, Key Eng. Mater. 169&170 (1999) 83.
[18] D.R. Clarke, Ultramicroscopy 4 (1) (1979) 33.
[19] A.V. Demin, Yu.I. Matyunin, A.S. Polyakov, M.I. Federova, in: Proceedings of the International Conference on Nuclear Waste Management and Environmental Remediation, Vol. 1, Prague, Czech Republic, 1993, p. 435.
[20] E. Gofuku, T. Ogama, H. Takasago, J. Appl. Phys. 66 (12) (1989) 6126.
[21] T. Nakano, K. Suzuki, T. Yamaguchi, J. Adhesion 46 (1994) 131.
[22] J. Mukerji, S.R. Biswas, Glass Technol. 12 (4) (1971) 107.
[23] C.C. Sartain, W.D. Ryden, A.W. Lawson, J. Non-Cryst. Solids 5 (1970) 55.
[24] Y.M. Chiang, L.A. Silverman, R.H. French, M. Cannon, J. Am. Ceram. Soc. 77 (5) (1994) 1143.
[25] M. Yamashita, T. Akai, H. Yamanaka, K. Sasage, private communication (2003).